10.1071/WF23098
International Journal of Wildland Fire

Supplementary Material

Spatial and temporal opportunities for forest resilience promoted by burn severity attenuation across a productivity gradient in north western Patagonia

Florencia Tiribelli[A,B,*], *Juan Paritsis*[A], *Iván Barberá*[A] and *Thomas Kitzberger*[A]

[A]INIBIOMA–Universidad Nacional del Comahue, CONICET, Quintral 1250, Bariloche 8400, Río Negro, Argentina

[B]Present address: Department of Forest and Conservation Sciences, Faculty of Forestry, University of British Columbia, Vancouver, BC V6T 1Z4, Canada

*Correspondence to: Email: flopitiribelli@gmail.com

Supplementary material 1.1 Burn severity classification

We trained a regional burn severity classification algorithm with field reference data and Landsat-based burn severity indexes to classify historic fires. Given the heterogeneity in species composition that our system has, we used several indices for the classification model to capture the variability in the spectral responses among vegetation types (Franco *et al.* 2020; Tran *et al.* 2020). Burn severity classification models are available for individual fires in some regions of Patagonia (Kitzberger *et al.* 2016; Mermoz *et al.* 2016, 2018; Franco *et al.* 2020), but a comprehensive burn severity classification across different fires, years and vegetation types has not yet been developed.

To do this we collected existing 302 georeferenced field control points of low (74), medium (86), and high (142) burn severity, across different vegetation covers for 6 of the 76 fires (Table S1, Table S2). These data were gathered in previous studies (Kitzberger *et al.* 2016; Landesmann *et al.* 2021) and in burn severity assessments form the Dirección de Lucha contra los Incendios Forestales y Emergencias (DLIFE) (Mermoz *et al.* 2008, 2016, 2018). We unified the field burn severity classification criteria and reclassified the data points to match those criteria (Table S3). We used these field control points as training data to build the algorithm and predict the burn severity patterns of all pixels in the 75 fires.

Table S1: Fires included in the model training

Fire	**Fire season**	**References**
Falso Granito	1998-99	(Landesmann *et al.* 2021)
Balcón del Gutierrez	1998-99	
Lolog	2007-08	(Mermoz *et al.* 2008)
Cholila	2014-15	(Kitzberger *et al.* 2016)
Alerces	2014-15	(Mermoz *et al.* 2016)
Alerces	2015-16	(Mermoz *et al.* 2018)

Table S2: Field fire severity data

Vegetation type	Low	Medium	High
Wet forest	31	19	9
Subalpine forest	10	33	16
Dry forest	8	7	20
Shrubland	25	27	97
Total	74	86	142

Table S3: Field sampling classification criteria

Fire severity	Litter	Shrubs	Tall trees
Low	Scorched	Fine fuels green or scorched. All shrubs alive.	Fine fuels and leaves green. All trees alive
Medium	Scorched or partially consumed	Fine fuels partially or totally consumed. Some scorched stems. Some alive.	Fine fuels brown, leaves sill in the canopy. Scorched stems. Few trees alive
High	Completely consumed	Fine and medium fuels totally consumed. Between scorched and burned stems All dead.	Fine fuels totally consumed. Between scorched and burned stems All trees dead.

Fine fuels: (< 6 mm diameter) Medium fuels: (between 6- and 20-mm diameter)

Remote sensing data and burn severity metrics calculations

We calculated nine Landsat-based burn severity metrics (Table S4; (Parks *et al.* 2018; Franco *et al.* 2020; Tran *et al.* 2020) in Google Earth Engine (GEE) (Gorelick *et al.* 2017) for each of the 75 fires in our fire database. W**Error! Bookmark not defined.**ithin GEE, for every fire and every burnt pixel we calculated the difference between the mean summer value (January – March) of each metric one year before (t-1) and after (t+1) the fire occurred: $index_t$ = mean (summer values)$_{t+1}$ – mean (summer values)$_{t-1}$. We only used summer pixels in order to avoid as much as possible clouds, snow cover and noise related to defoliation in deciduous communities. We used the whole Landsat Surface Reflectance Tier 1 datasets (4, 5, 7 and 8), and excluded pixels with clouds, shadow, water, or snow based on the quality assessment band (see (Parks *et al.* 2018). As the images were obtained from different Landsat sensors (TM, ETM+ and OLI), we transformed the reflectance values to the OLI scale (Roy *et al.* 2016).

Table S4: Satellite-based burn severity metrics

Burn severity index	Formula	References
Normalised Difference Vegetation Index (NDVI)	$NDVI = \frac{NIR - RED}{NIR + RED}$	(Tran *et al.* 2020)
Normalised Burn Ratio (NBR)	$NBR = \frac{NIR - SWIR2}{NIR + SWIR2}$	(Parks *et al.* 2018; Long *et al.* 2019; Tran *et al.* 2020)
Normalised Difference Water Index (NDWI)	$NDVI = \frac{NIR - SWIR1}{NIR + SWIR1}$	(Tran *et al.* 2020)
Burned Area Index (BAI)	$BAI = \frac{1}{(0.1 + RED)^2 + (0.06 + NIR)^2}$	(Long *et al.* 2019; Tran *et al.* 2020)
Mid InfraRed Burn Index (MIBI)	$MIRBI = 10 \times SWIR2 + 9.8 \times SWIR1 + 2$	(Long *et al.* 2019; Tran *et al.* 2020)
Char Soil Index (CSI)	$CSI = \frac{NIR}{SWIR}$	(Tran *et al.* 2020)
Normalized Burn Ratio 2 (NBR2)	$NBR = \frac{SWIR1 - SWIR2}{SWIR2 + SWIR2}$	(Long *et al.* 2019)
Relativized Burn Ratio (RBR)	$RBR = \frac{(\mathrm{NBR}_{prefire} - NBR_{postfire})}{\mathrm{NBR}_{prefire} + 1.001}$	(Long *et al.* 2019)
Soil adjusted Vegetation index (SAVI)	$SAVI = \frac{1.5 \times (NIR - RED)}{NIR + RED + 0.5}$	(Long *et al.* 2019)

Fire severity classification algorithm

To classify burn severity from the spectral burn severity metrics we first extracted the values of the nine satellite severity metrics for every field point and calculated a correlation matrix with the *cor* function of the stats package in R 4.0.2. In order to assess the level of separability among classes for every severity metric we calculated a separability index (SI, (Kaufman and Remer 1994).

$$SI_{12} = \frac{|\mu_1 - \delta_2|}{\delta_1 + \delta_2}$$

where μ_1 and μ_2 are the mean values of the considered burn severity metrics of two consecutive severity classes and δ_1 and δ_2 are the corresponding standard deviations.

The separability among high and medium burn severity was poor for every metric, thus we calculated the separability index among low and high severity classes (Table S5, see also

(Franco *et al.* 2020). Given that the separability index between low and high severity was better, we removed every point of the medium field-based burn severity class from the study and built a classifier for low and high severity. This decision makes also ecological sense as even in moderate severities fire sensitive species are killed, meaning that ecological implications are analogous (Landesmann *et al.* 2021; Franco *et al.* 2022).

Table S5: Separability index among low and high burn severity for the nine different burn severity metrics

Metric	All fuel types	Shrubland	Wet Forest	Subantarctic forest	Dry forest	All forest types
dNBR	0.414	0.233	0.957	0.470	0.643	0.650
dNBR2	0.608	0.394	1.07	0.784	0.787	0.781
dNWI	0.146	0.005	0.794	0.186	0.51	0.421
dMIRBI	0.772	0.678	1.08	0.968	0.661	0.919
dBAI	0.031	0.233	0.389	0.110	0.399	0.195
dSAVI	0.152	0.079	0.637	0.238	0.352	0.335
dCSI	0.019	0.067	0.671	0.051	0.341	0.240
drbr	0.503	0.318	0.947	0.582	0.633	0.728

After evaluating the correlation matrix and the separability indexes we chose the best three metrics, dNBR2, dNWI, dMIRBI and fitted a Bayesian logistic model with the function *stan_glm* of the package rstanarm (Brilleman *et al.* 2018; Goodrich *et al.* 2020) in R (R Core Team 2020). When training a burn severity classification algorithm, it is common to include variables such as vegetation cover and topography, but as the aim of the study was to assess the importance of those variables as burn severity drivers, we needed to fit a severity classifier independent of them. To fit the model, we first divided the data into a training (70%) and a test (30%) set. After fitting the model, we checked for convergence and the effective sample size before performing a posterior predictive check. We also contrasted the model against a baseline model using WAIC.

To validate the trained model, we classified the test set and compared the predicted response to the actual data with a confusion matrix, and calculated the accuracy, kappa sensitivity and specificity statistics functions *predict* and *confusionMatrix* of the caret package (Kuhn 2020) in R 4.0.2 (R Core Team 2020). As a point prediction of the high severity probability, we used its posterior median. As the logistic model predicts probabilities and not classes (low and high), we

did this for different probability cut-offs that produced a classification of low and high fire severity and chose the one that produced high values of all 4 statistics. We then classified the 76 fires severity patterns with the validated model using the *predict* function of caret package (Kuhn 2020) in R 4.0.2 (R Core Team 2020).We saved both, the maps with the burn severity probability from the logistic model and the maps classified into low and high burn severity with the chosen probability cut-off (Figure S1).

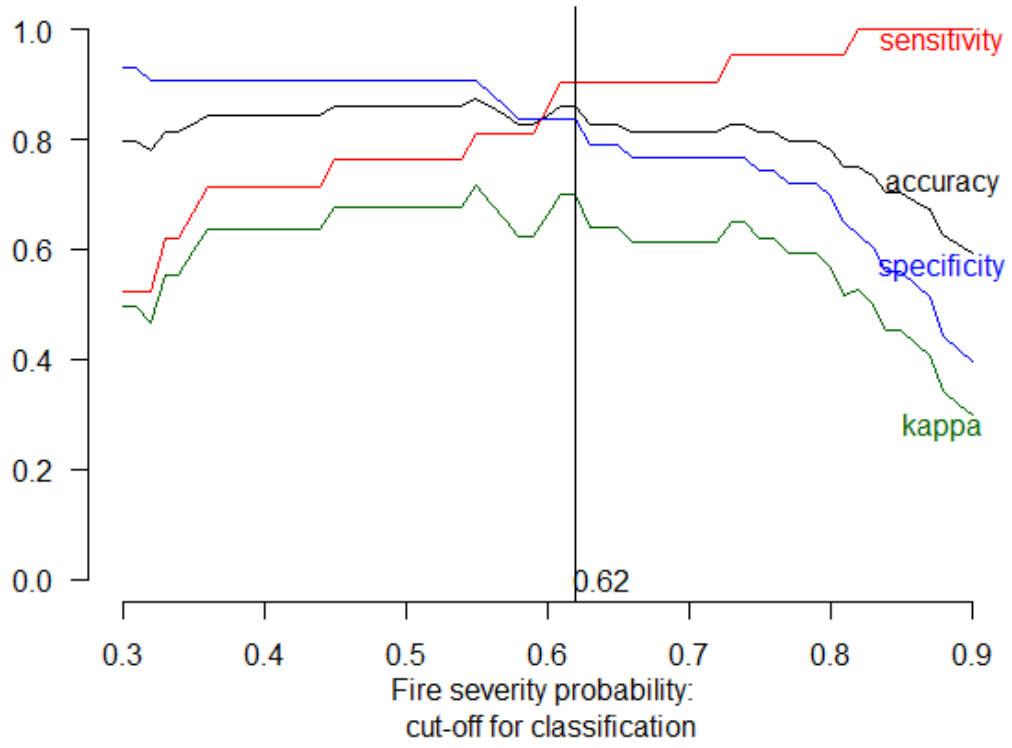

Figure S1: Out of sample Accuracy, Kappa, Specificity and Sensitivity values against a range of fire severity probability cut-offs.

Table S6: Fire severity classification summary

Fire_ID	Wet forest	Subalpine forest	Dry forests	Shrubland	Exotic Forest
Alerces2015	0.80	0.92	0.72	0.99	
Alerces2016	0.84	0.92	0.96	0.99	1.00
AltoChubut11				0.50	
AltoChubut16		1.00		0.57	
BalconGutierrez	0.41	0.72	0.98	0.96	
Cholila_2015	0.83	0.88	0.87	0.94	0.85
CoCampana	0.94	1.00		1.00	
CoCarbon			1.00	0.98	1.00
CoDormilon	0.92	0.92		0.99	
CoVentana		1.00		0.99	0.96
CrucedeMaiten			1.00	1.00	0.98
currchico_FEB2016		1.00		1.00	
Currumahuida	0.98	0.97	0.96	0.94	0.93
Epuyen00	0.05	0.53	0.30	0.30	0.14
Epuyen01	0.31		0.57	0.88	0.75
Epuyen02		0.73	0.80	0.64	0.22
Epuyen04				0.94	
Epuyen06			1.00	0.97	0.89
Espejo	0.88				
Esperanza	0.72	0.52	0.96	0.93	
FalsoGranito	0.71	0.80	0.84	0.98	1.00
Golondrinas02			0.55	0.48	0.50
LagoPuelo-Epuyen00	1.00	0.83		0.96	
LagVerde_FEB2008		0.91			
Lolog_2008	0.16	0.65		0.95	
Lolog2002		0.95	0.93	0.99	
LosRepollos_CuestadelTernero		0.84	0.93	0.97	0.92
Machonico99				0.96	0.98
modland_2002_Epuyen	0.97		0.92	0.99	0.97
modland_2002_FoyelE		1.00		1.00	
modland_2002_LosRepollosNE		0.95		0.97	
modland_2004_LosRepollosSE		1.00		1.00	
modland_2005_CholilaS		1.00	1.00	1.00	
modland_2008_EpuyenE				0.99	1.00
modland_2008_EsquelO		0.57	0.67	0.98	0.79
modland_2009_TromenS		1.00	0.97	1.00	
modland_2011_HoyoNO	0.67		0.64	0.90	0.95
modland_2012_HoyoSE	0.97	1.00	0.90	0.98	0.95
modland_2012_LagoEpuyenN	0.92	0.82	0.90	0.95	0.93
modland_2012_LagoRosarioS		0.94		0.98	
modland_2014_RioPicoSO		0.00		1.00	
modland_2015_LagoHuechulafquenS	0.81	0.84	0.98	0.99	
modland_2015_LagoNahuelHuapiN			0.99	1.00	
modland_2016_LagoPalenaS		0.86		0.98	1.00
modland_2016_RioPicoSOa		0.95		0.97	1.00
modland_2016_RioPicoSOb		0.87		0.98	

modland_2016_RioPicoSOc	0.91	0.97		0.96	
modland_2016_RioPicoSOd	0.80	0.73		0.91	
modland_2016_TrevelinS			0.96	0.99	1.00
modland_2018_RioPonchoMoro	0.96		0.99	1.00	1.00
modland_2019_EpuyenSE			1.00	1.00	1.00
PalomaBlanca		0.88	1.00	0.98	0.96
Patriada	0.89		0.67	0.74	0.19
Patriada03			0.98	1.00	1.00
Patriada11	0.28		0.69	0.88	0.49
Patriada12	0.68		0.50	0.76	0.71
RioHermoso_OCT2011				0.93	0.50
Ruiz_Lostra			0.77		
SierraChata		0.59		0.91	
Splif1999		0.54		0.95	1.00
TK1999_1			0.50	0.95	
TK1999_2	0.64	0.60		0.54	
TK1999_3	0.54		0.90	0.98	1.00
TK1999_4			0.91	0.99	0.99
TK1999_5	0.97	1.00		1.00	
TK2000_1					0.40
TK2000_2				0.21	0.33
TK2000_3					0.64
TK2004_1	1.00	1.00		1.00	
TK2004_2				0.99	
Turbio00		0.44		0.50	
Turbio02	0.56	0.58	0.42	0.77	
Turbio15	0.93	0.92	0.99	0.93	
Turbio16	0.94	0.96		0.96	
Mean	0.75	0.82	0.84	0.90	0.81
Standard deviation	0.26	0.21	0.19	0.17	0.27
Maximum	1.00	1.00	1.00	1.00	1.00
Minimum	0.05	0.00	0.30	0.21	0.14

Table S7: List of variables used to explain the drivers of burn severity in the landscape.

Covariate (units)	Resolution	Source
Topography/Physical		
Elevation (m asl)	30 m	NASA SRTM Digital Elevation
Slope (°)	30 m	NASA SRTM Digital Elevation
Northerliness	30 m	NASA SRTM Digital Elevation
Easterliness	30 m	NASA SRTM Digital Elevation
Distance to nearest fire edge	30 m	
Distance to the nearest water body	30 m	
Climate		
Annual precipitation BIO12 (°C)	30 arc sec	Fick & Hijmans (2017) (WorldClim2.0)
Annual mean temperature BIO1 (°C)	30 arc sec	Fick & Hijmans (2017) (WorldClim2.0)
Land Cover		
Vegetation (4 classes)	30 m	WWF Valdivian Ecoregion Vegetation (Lara et al. 1999)
Normalized difference vegetation index*	30 m	
Google Earth vegetation mapping (6 classes)	30 m	
Fire weather		
Summer (Dec-Feb) Temperature anomaly (std)	1/24 deg	TerraClimate (Abatzoglou et al. 2018)
Summer (Dec-Feb) Palmer drought severity index (std)	1/24 deg	TerraClimate (Abatzoglou et al. 2018)

*Calculated as the mean NDVI of every valid record available during the pre-fire summer season (Dec-Feb) in Google Earth Engine.

References

Brilleman S, Crowther M, Moreno-Betancur M, Buros Novik J, Wolfe R (2018) Joint longitudinal and time-to-event models via Stan. StanCon 2018. 10-12 Jan 2018. Pacific Grove, CA, USA. https://github.com/stan-dev/stancon_talks/.

Franco MG, Mundo IA, Veblen TT (2020) Field-validated burn-severity mapping in North Patagonian forests. *Remote Sensing* **12**, 1–18. doi:10.3390/rs12020214.

Franco MG, Mundo IA, Veblen TT (2022) Burn severity in Araucaria araucana forests of northern Patagonia: tree mortality scales up to burn severity at plot scale, mediated by topography and climatic context. *Plant Ecology*. doi:10.1007/s11258-022-01241-w.

Goodrich B, Gabry J, Ali I, Brilleman S (2020) rstanarm: Bayesian applied regression modeling via Stan. R package version 2.21.1. https://mc-stan.org/rstanarm.

Gorelick N, Hancher M, Dixon M, Ilyushchenko S, Thau D, Moore R (2017) Remote Sensing of Environment Google Earth Engine : Planetary-scale geospatial analysis for everyone. *Remote Sensing of Environment* **202**, 18–27. doi:10.1016/j.rse.2017.06.031.

Kaufman YJ, Remer LA (1994) Detection of Forests Using Mid-IR Reflectance: An Application for Aerosol Studies. *IEEE Transactions on Geoscience and Remote Sensing* **32**, 672–683. doi:10.1109/36.297984.

Kitzberger T, Grosfeld J, Gowda JH, Gonzalez Musso R, Iglesias A, Landesmann JB, Tiribelli F (2016) Diagnóstico de la severidad de fuego y propuestas de restauración y manejo a nivel predial para áreas afectadas por el incendio de Cholila de 2015.

doi:10.13140/RG.2.2.17033.24169.

Kuhn M (2020) caret: Classification and Regression Training. R package version 6.0. 86. https://cran.r-project.org/package=caretNo Title.

Landesmann J, Tiribelli F, Paritsis J, Veblen TT, Kitzberger T (2021) Increased fire severity triggers positive feedbacks of greater vegetation flammability and favors plant community-type conversions (B Collins, Ed.). *Journal of Vegetation Science* **32**, 1–13. doi:10.1111/jvs.12936.

Long T, Zhang Z, He G, Jiao W, Tang C, Wu B, Zhang X, Wang G, Yin R (2019) 30m resolution global annual burned area mapping based on landsat images and Google Earth Engine. *Remote Sensing* **11**, 1–30. doi:10.3390/rs11050489.

Mermoz M, Müller M, Nuñez C, Pastore H, Eduardo R (2016) Evaluación ecológica del incendio El Cristo en el área Futalaufquen del Parque Nacional los Alerces. Administración de Parques Nacionales. Dirección de Lucha contra Incendios Forestales. Dirección Regional Patagonia Norte. Parque Nacional Los Alerces.

Mermoz M, Müller M, Presti P, Schinelli L, Withington T (2018) Informe final de la evaluación del efecto del fuego sobre la vegetación afectada por el incendio Cañadón del arroyo cascada en enero de 2016. Administración de Parques Nacionales. Dirección de Lucha contra Incendios Forestales. Dirección Regional Patagoni.

Mermoz M, Sanguinetti J, Kitzberger T, Lara M, García L (2008) Evaluación ecológica de los daños ocasionados por los incendios forestales del área de Lolog – Parque Nacional Lanín – Febrero-Aril de 2008. Administración de Parques Nacionales, Parque Nacional Lanín – Delegación Regional Patagonia.

Parks SA, Holsinger LM, Voss MA, Loehman RA, Robinson NP (2018) Mean composite fire severity metrics computed with google earth engine offer improved accuracy and expanded mapping potential. *Remote Sensing* **10**, 1–15. doi:10.3390/rs10060879.

R Core Team (2020) R: A language and environment for statistical computing. R Foundation for Statistical Computing,Vienna, Austria. doi:ISBN 3-900051-07-0.

Roy DP, Zhang HK, Ju J, Gomez-Dans JL, Lewis PE, Schaaf CB, Sun Q, Li J, Huang H, Kovalskyy V (2016) A general method to normalize Landsat reflectance data to nadir BRDF adjusted reflectance. *Remote Sensing of Environment* **176**, 255–271. doi:10.1016/j.rse.2016.01.023.

Tran BN, Tanase MA, Bennett LT, Aponte C (2020) High-severity wildfires in temperate Australian forests have increased in extent and aggregation in recent decades. *PLoS ONE* **15**,. doi:10.1371/journal.pone.0242484.

Supplementary material 1.2 Regression analysis

Model results

Table S8:

Covariate	Parameter	mean	sd	f	Rhat	n.eff
Intercept	μ^{a0}	2.138	0.082	1.00	1.000	8170
Distance to fire edge	a1	0.338	0.017	1.00	1.000	6303
NDVI	a1	-0.058	0.017	1.00	1.002	1669
Slope	a1	-0.131	0.015	1.00	1.000	11768
Northing	a1	0.265	0.017	1.00	1.000	4364
Easting	a1	0.346	0.018	1.00	1.000	15268
Distance to water bodies	a1	0.034	0.012	1.00	1.000	9022
Annual precipitation	a1	-0.163	0.017	1.00	1.001	2110
Annual mean temperature	a1	0.003	0.014	0.59	1.001	3080
Distance to fire edge	a2	-0.141	0.012	1.00	1.001	5009
NDVI	a2	-0.053	0.008	1.00	1.002	1247
Slope	a2	0.066	0.011	1.00	1.000	18000
Distance to water bodies	a2	-0.021	0.013	0.95	1.001	3583
Annual precipitation	a2	0.073	0.012	1.00	1.000	9267
Annual mean temperature	a2	-0.034	0.01	1.00	1.000	7805
Variance between random effects	σ^{a0}	0.257	0.066	1.00	1.000	18000

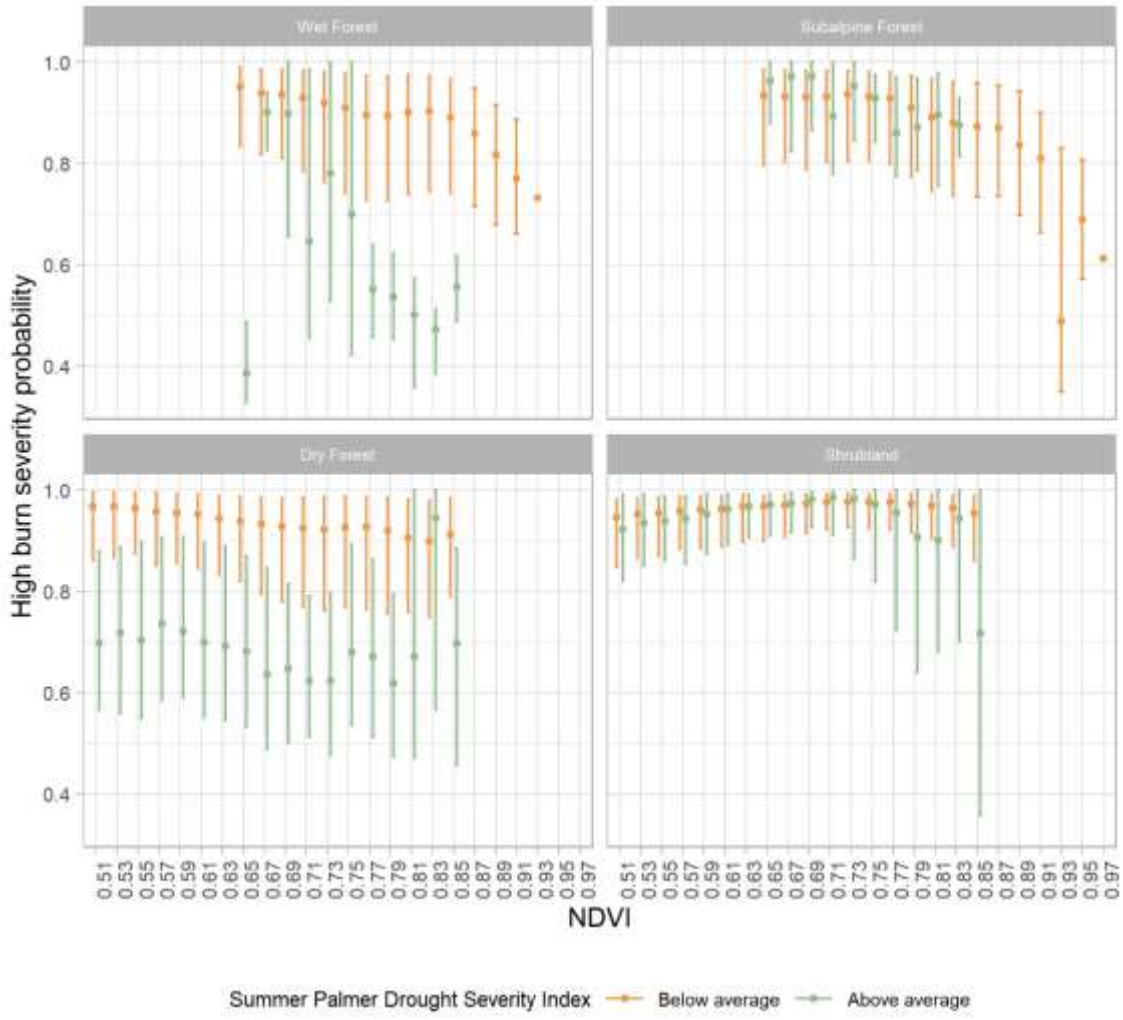

Figure S2: High burn severity probability as a function of NDVI for different vegetation types and under different Palmer Drought Severity Index anomalies scenarios. Points correspond to median values and the lower and upper whiskers extend to $1.5 \times \frac{IQR}{\sqrt{n}}$ (IQR: inter-quartile range).

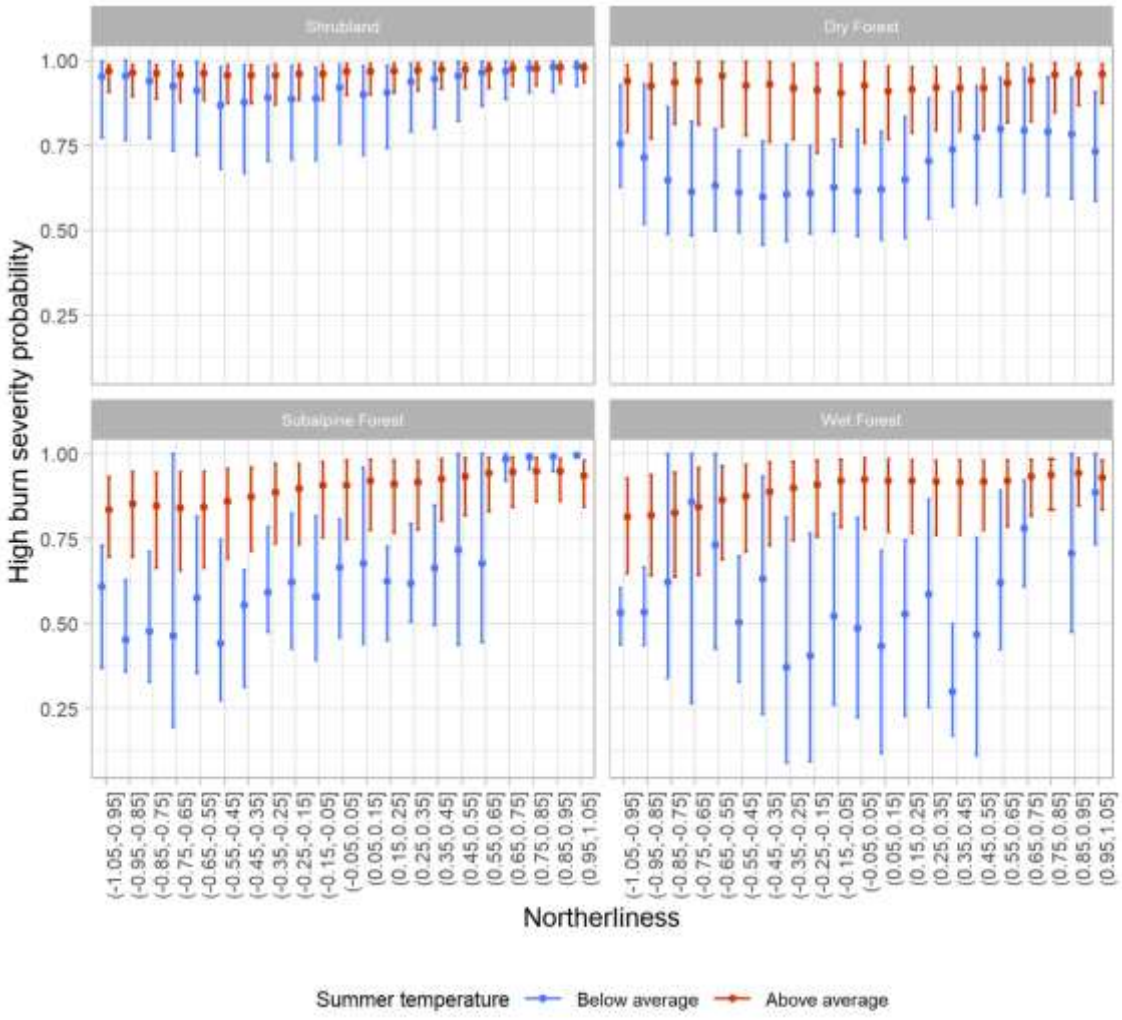

Figure S3: High burn severity probability as a function of Northerliness for different vegetation types and under different summer temperature anomalies scenarios. Points correspond to median values and the lower and upper whiskers extend to $1.5 \times \frac{IQR}{\sqrt{n}}$ (IQR: inter-quartile range).

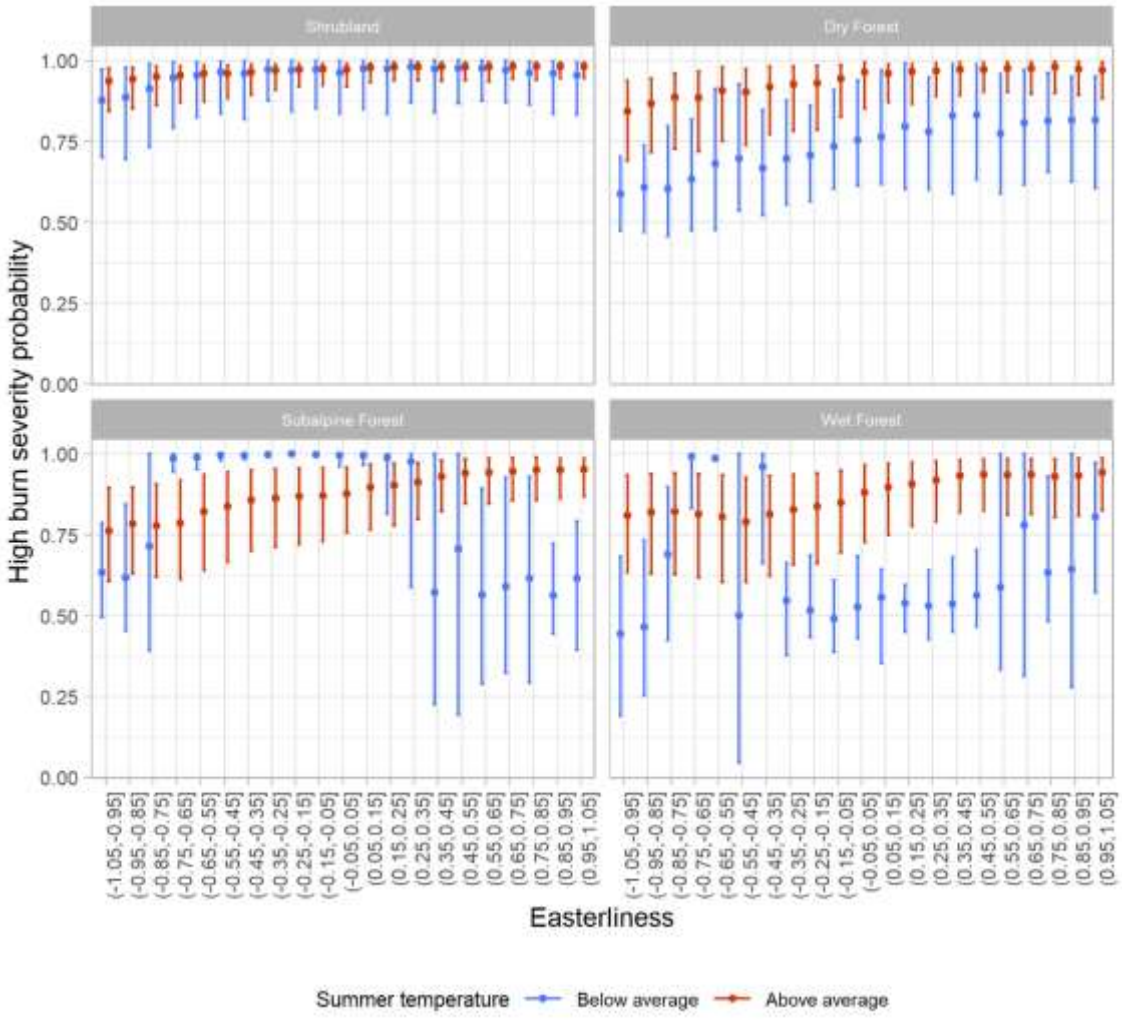

Figure S4: High burn severity probability as a function of Easterliness for different vegetation types and under different summer temperature anomalies scenarios. Points correspond to median values and the lower and upper whiskers extend to $1.5 \times \frac{IQR}{\sqrt{n}}$ (IQR: inter-quartile range).